6-2010

Conditions for Thrust Faulting in a Glacier

Peter Lindsay Moore
Iowa State University, pmoore@iastate.edu

Neal R. Iverson
Iowa State University, niverson@iastate.edu

Denis Cohen
Iowa State University, dcohen@iastate.edu

Conditions for Thrust Faulting in a Glacier

Abstract
Dipping, arcuate bands of debris-rich ice outcropping near the margins of glaciers are often interpreted as thrust faults, assumed to originate in zones of longitudinal compression. Identification of thrusts is typically based either on the geometry and sedimentology of the debris bands or on the crystal fabric of surrounding ice, but the physical processes necessary to generate thrusts are rarely evaluated. Herein, we combine a numerical model of compressive ice flow near a glacier margin with theoretical stress and strain rate criteria for ice fracture and stress criteria for frictional slip to determine the conditions necessary for thrust faulting in glaciers. This model is applied to two different glaciological settings where longitudinal compression has been documented: (1) the transition between warm-based and cold-based ice near the terminus of Storglaciären, Sweden, and (2) the downglacier extent of the 1983 surge front of Variegated Glacier where surging ice encountered stagnant ice. Simulations representing the margin of Storglaciären indicate that peak compressive strain rates are six orders of magnitude too small to induce fracture, whereas at Variegated Glacier, strain rates were an order of magnitude too small for compressive fracture. In both groups of simulations, preexisting fractures governed by Coulomb friction are susceptible to slip if they span the ice thickness, are oriented close to the optimal fracture angle, and, in the case of Storglaciären, are subject to water pressures that are a large fraction of ice overburden pressure. Variations about the optimal fracture orientation, low or zero water pressure, high sliding friction coefficient, and limited vertical or lateral fracture extent each tend to suppress thrusting.

Keywords
glacier, mechanics, faulting, Storglaciären, Variegated Glacier

Disciplines
Glaciology | Natural Resources Management and Policy

Comments
This article is from *Journal of Geophysical Research: Earth Surface* 115 (2010): art. F02005, doi:10.1029/2009JF001307. Posted with permission.

JOURNAL OF GEOPHYSICAL RESEARCH, VOL. 115, F02005, doi:10.1029/2009JF001307, 2010

Conditions for thrust faulting in a glacier

Peter L. Moore,[1] Neal R. Iverson,[1] and Denis Cohen[1]

Received 13 March 2009; revised 17 August 2009; accepted 16 October 2009; published 10 April 2010.

[1] Dipping, arcuate bands of debris-rich ice outcropping near the margins of glaciers are often interpreted as thrust faults, assumed to originate in zones of longitudinal compression. Identification of thrusts is typically based either on the geometry and sedimentology of the debris bands or on the crystal fabric of surrounding ice, but the physical processes necessary to generate thrusts are rarely evaluated. Herein, we combine a numerical model of compressive ice flow near a glacier margin with theoretical stress and strain rate criteria for ice fracture and stress criteria for frictional slip to determine the conditions necessary for thrust faulting in glaciers. This model is applied to two different glaciological settings where longitudinal compression has been documented: (1) the transition between warm-based and cold-based ice near the terminus of Storglaciären, Sweden, and (2) the downglacier extent of the 1983 surge front of Variegated Glacier where surging ice encountered stagnant ice. Simulations representing the margin of Storglaciären indicate that peak compressive strain rates are six orders of magnitude too small to induce fracture, whereas at Variegated Glacier, strain rates were an order of magnitude too small for compressive fracture. In both groups of simulations, preexisting fractures governed by Coulomb friction are susceptible to slip if they span the ice thickness, are oriented close to the optimal fracture angle, and, in the case of Storglaciären, are subject to water pressures that are a large fraction of ice overburden pressure. Variations about the optimal fracture orientation, low or zero water pressure, high sliding friction coefficient, and limited vertical or lateral fracture extent each tend to suppress thrusting.

Citation: Moore, P. L., N. R. Iverson, and D. Cohen (2010), Conditions for thrust faulting in a glacier, *J. Geophys. Res.*, *115*, F02005, doi:10.1029/2009JF001307.

1. Introduction

[2] Thrusting of bed-derived sediment from the bottom of a glacier to its surface may be an important mechanism of sediment transport [e.g., *Alley et al.*, 1997] (Figure 1). Thrusting may also result in unique suites of landforms indicative of supraglacial debris accumulation near an ablating ice margin [e.g., *Hambrey et al.*, 1997]. The observation of seams of indurated diamicton along upglacier-dipping, arcuate surfaces outcropping near glacier termini is taken by some as evidence of widespread thrusting [*Hambrey et al.*, 1999]. Debris-bearing surfaces with evident dip-slip offsets observed in tunnels or marginal ice exposures are also viewed as further evidence that thrusting is important and ubiquitous.

[3] However, several authors have argued that development of thrust faults in grounded glacier ice should be mechanically inhibited [e.g., *Weertman*, 1961; *Hooke*, 2005]. Among the key difficulties cited is the comparatively large strain rate necessary to produce macroscopic compressive fractures in ice [*Paterson*, 1994]. Large strain rates are necessary to exceed the rate at which strain can be accommodated by ductile flow at the tips of small preexisting cracks [e.g., *Schulson*, 2001]. This problem can be surmounted, to some extent, by assuming that a thrust fault exploits a preexisting weakness in the ice such as a crevasse trace.

[4] In this paper, we combine a 2-D, steady state numerical model of ice flow over a slip to no-slip transition (SNST) at the bed with criteria describing two possible mechanisms for thrust faulting: development of compressive fractures in initially homogeneous ice, and reactivation of a preexisting and pervasive fracture. Attention is focused on conditions relevant to SNSTs in the termini of grounded glaciers, arising either from thermal transitions at the glacier bed or from transients associated with surges. The intent is not to model the evolution of fractures in time but to find the conditions under which either fracture or frictional slip can be initiated, since this is a prerequisite for the development of debris-bearing thrust faults.

2. Background

2.1. Field Observations

[5] We are aware only of a single case in which the evidence for thrust faulting in a glacier is unequivocal. Folding, buckling, and faulting were observed near the

[1]Department of Geological and Atmospheric Sciences, Iowa State University, Ames, Iowa, USA.

0148-0227/10/2009JF001307

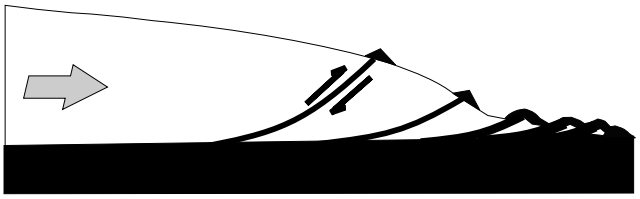

Figure 1. Schematic illustration of terminal thrust faults and consequent accumulation of bed-derived debris at the ice surface.

terminus of Variegated Glacier, Alaska, during its surge in 1983 [*Raymond et al.*, 1987]. Propagation of the surge into stagnant marginal ice produced peak compressive strain rates several orders of magnitude larger than typical non-surge strain rates in that part of the glacier [*Kamb et al.*, 1985; *Sharp et al.*, 1988]. Thrust faults dipping ~40° upglacier accounted for as much as 50% of local shortening and developed approximately parallel to the preexisting foliation pattern in the ice. Some thrusts were small and resulted in only a few meters of offset at the surface, while others were much larger, accumulated large displacements, and cut through the downglacier limbs of large bulge folds that preceded them [*Sharp et al.*, 1988]. Measured vertical displacements at the ice surface were larger than those calculated from horizontal displacements assuming incompressible ice, suggesting that englacial or subglacial water-filled voids were opening during the passage of the surge front [*Raymond et al.*, 1987, p. 9048].

[6] Observations at a number of polythermal surge-type glaciers also point toward faulting associated with propagation of a surge front into ice at a frozen margin, although the interpretation of fault structures is often more equivocal in these cases. *Clarke and Blake* [1991] made several observations on Trapridge Glacier suggesting that a growing bulge in the ice surface was associated with the growth of an englacial debris-rich discontinuity. This feature also coincided with a reversal in the temperature profile, suggesting that warm basal ice beneath the bulge was being uplifted along this discontinuity over colder, slower-moving ice ahead of the bulge. Although no actively slipping fault ever intersected the surface at Trapridge, upglacier-dipping, debris-rich structures that could be interpreted as thrust faults were later observed in the stagnant ice closer to the terminus (J. Shaw, unpublished data, 2008). *Hambrey et al.* [1996] and *Murray et al.* [1998] describe bands of ice-bearing bed-derived debris emerging in the vicinity of the transition between temperate and cold-based ice at Bakaninbreen, a surge-type polythermal glacier in Svalbard. Ground-penetrating radar [*Murray et al.*, 1998] and seismic surveys [*Smith et al.*, 2002] showed that some of these structures continued to depth and intersected the bed near the thawed/frozen transition, which coincided with the downglacier extent of a surge that lasted from 1985 until 1995 [*Smith et al.*, 2002]. However, some features once described as thrusts in similar polythermal surge-type glaciers have been reinterpreted as basal crevasse-fill structures [*Woodward et al.*, 2002; *Glasser et al.*, 2003a; *Woodward et al.*, 2003].

[7] In nonsurge-type glaciers, similar features outcropping in glacier termini have been ascribed to thrust faulting. For example, structures with many of the characteristics attributed to thrusting have been described in marginal ice in Greenland [*Bishop*, 1957], Alaska [*Rabus and Echelmeyer*, 1997], Sweden [*Glasser et al.*, 2003b], New Zealand [*Kirkbride and Spedding*, 1996], Switzerland [*Herbst and Schopfer*, 2006], and Canada [*Goldthwait*, 1951; *Hambrey and Muller*, 1978]. In Sweden, for example, *Glasser et al.* [2003b] examined debris bands outcropping on the surface of Storglaciären, where typical ice surface velocities are on the order of 10 m a^{-1} [*Jansson et al.*, 2000] and strain rates are at least three orders of magnitude smaller than at the surge front on Variegated Glacier. Nevertheless, *Glasser et al.* [2003b] interpreted sediment characteristics, isotopic data, and radar surveys to indicate that these bands continued all the way to the bed, and hence were the products of thrusting.

[8] Despite widespread reports of thrusts, some researchers have questioned the interpretation of many of these structures. For example, some debris-bearing planar structures may be inherited from the primary stratigraphy of the ice [e.g., *Hooke and Hudleston*, 1978] and others may be sediment-filled surface [*Bennett et al.*, 2000] or bottom [*Ensminger et al.*, 2001; *Woodward et al.*, 2002] crevasses that are subsequently rotated into upglacier-dipping orientations. Other debris bands have been interpreted as basal ice that appears enclosed in ice because of overriding of marginal aprons of superimposed ice [*Hooke*, 1973]. Similar features have also been interpreted as glaciofluvial deposits from englacial flows [*Kirkbride and Spedding*, 1996].

[9] Evidence supporting thrusting in glaciers is not limited to field observations. Mathematical models of ice flow suggest that abrupt transitions in basal drag can produce large stress concentrations in the ice, perhaps sufficient to cause fracture [e.g., *Hutter and Olunloyo*, 1980; *Lliboutry*, 2002]. In fact, these models predict infinite deviatoric stresses at the SNST. However, such a result is untenable because infinite stresses cannot be supported by ice. Furthermore, there are several mechanisms that likely reduce the abruptness of the transition in basal drag, and thereby reduce the magnitude of stress concentrations [e.g., *Fowler et al.*, 2001; *Moore et al.*, 2009]. The extent to which the basal drag transition is smoothed out in the general case is unknown, so for the simulations described hereinafter, we adopt the assumption of an abrupt transition.

2.2. Flow of Ice

[10] Under stress fields typical of glaciers, ice behaves in a largely ductile manner. While crevasses are clear evidence of ice fracturing in tension, the compressive strength of ice is considerably larger [e.g., *Schulson*, 2001]. Glen's law, the constitutive relation that best describes the flow of glacier ice, is

$$\dot{\varepsilon}_e = \left(\frac{\tau_e}{B}\right)^n, \tag{1}$$

where $\dot{\varepsilon}_e$ and τ_e are the effective strain rate and effective shear stress, respectively, and B is a viscosity parameter [*Hooke*, 2005]. The flow law exponent n is thought to range from 1 to 4, depending on the stress regime. While a

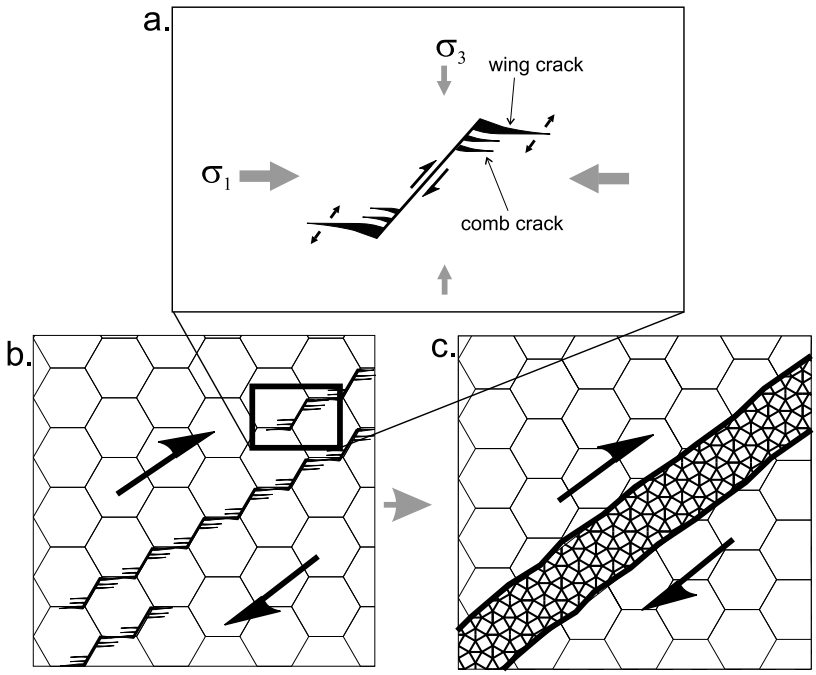

Figure 2. Development of macroscopic fracture zones by propagation and linkage of grain-scale flaws. (a) Single sliding crack under differential stress showing opening-mode wing cracks and comb cracks. (b) Schematic depiction of linkage of multiple cracks. (c) Failure of slender columns of ice bounded by comb cracks, creating a damage zone and macroscopic fracture. After *Schulson* [2001].

composite value of 3 is usually used for simplicity, in circumstances where deviatoric stresses are large, higher values of n may be appropriate. Such strongly nonlinear behavior can lead to significant strain localization, and this can be further exaggerated if impurities (e.g., sparse sediment particles) or crystal fabrics soften discrete layers. Nevertheless, under the right circumstances, ice is known to fracture in laboratory shear and compression tests [e.g., *Rist and Murrell*, 1994].

2.3. Failure Criteria

[11] Glacier ice, like other natural polycrystalline materials, is rich in microscopic flaws such as voids, inclusions, and cracks. These small flaws normally do not disrupt the macroscopic ductile behavior, but can play an important role in fracture under some circumstances. No matter what the expected mode of failure is, optimally oriented flaws and preexisting discontinuities will likely be the locus of fault development. Shear failure requires overcoming frictional resistance for the initiation of slip along an incipient crack or slip surface. Assuming no cohesive strength, the general expression for the shear stress τ_y sufficient to initiate slip is the simple Coulomb criterion $\tau_y = \mu\sigma_n$, where σ_n is the stress normal to the sliding surface and μ is the coefficient of static friction. A prerequisite to brittle compressive fracture of ice is slip either along grain boundaries or preexisting cracks and the formation of slip-accommodating wing cracks where local tensile stresses develop at crack tips [*Schulson*, 2001] (Figure 2a). Adjacent to wing cracks may be subsidiary "comb cracks," which isolate slender columns of ice near the tips of incipient sliding cracks. When brittle failure takes place, it is by the failure of these columns and linkage of neighboring wing cracks, creating a continuous zone of damage (Figures 2b and 2c). However, even if the shear stress is sufficient to cause crack-interface slippage, crack growth will be inhibited if the strain rate is small enough that strain at crack tips can be accommodated by ductile ice flow. Thus, fracture of ice in compression is a complex function of the applied principal stresses, frictional properties of the ice, rheological behavior of the ice, and geometry of the crack system. Theoretical expressions for the criteria that must both be independently met for brittle fracture are described by *Renshaw and Schulson* [2001] and *Schulson* [2001]:

$$\dot{\varepsilon}_{B/D} = \frac{2(3/2)^{(n-(1/2))}(n+1)^2 B^* K_{Ic}^3}{c^{n/2} n\sqrt{\pi}[(1-R)-\mu(1+R)]} \tag{2}$$

$$\sigma_f = \frac{2K_{Ic}}{\left[\left(1+\left(1-\mu\frac{1+R}{1-R}\right)^{2/3}\right)^{1/2}-1\right]^{1/2}\left[1+3\mu^2\alpha^2(1-R)^2\right]^{1/2}c^{1/2}}, \tag{3}$$

where $\dot{\varepsilon}_{B/D}$ is the strain rate corresponding to the ductile-brittle transition, σ_f is the yield strength of crack-bounding ice, B^* is a fluidity parameter related to B (such that $B^* = B^{-n}$), K_{Ic} is the fracture toughness of ice, c is half the characteristic ice crystal diameter, α is the length-to-width ratio of the columns of ice bounded by comb cracks, and $R = \sigma_3/\sigma_1$, the principal stress ratio. Herein, σ_1 is the most compressive principal stress and σ_3 is the least

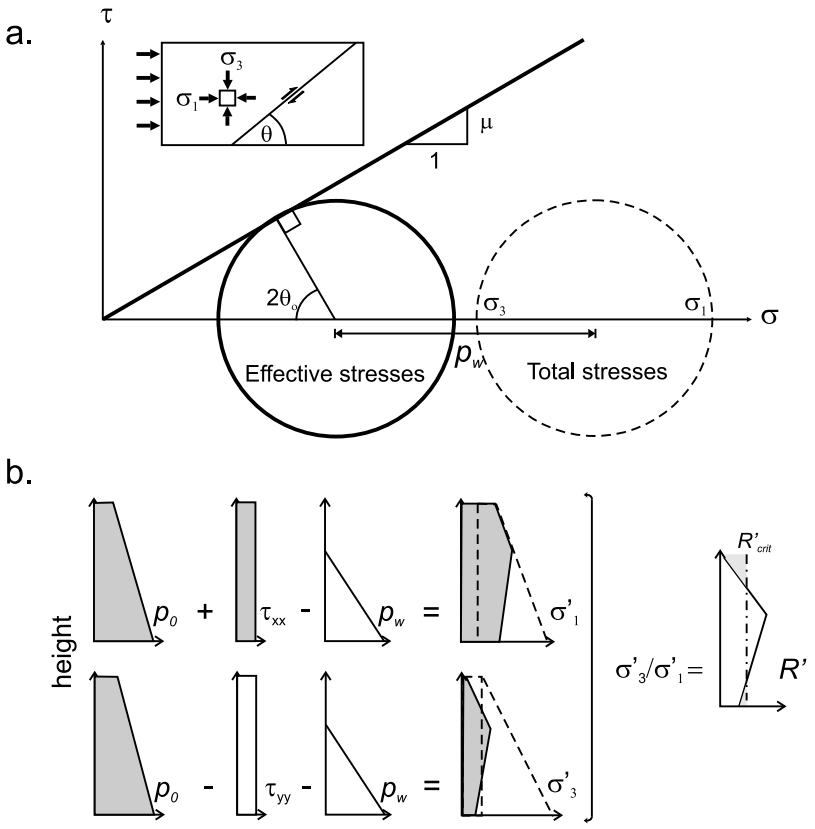

Figure 3. Illustration of the Coulomb criterion for slip on a fracture oriented at an angle θ to the most compressive stress. (a) Mohr circle illustration of effect of water pressure on principal stresses see *Scholz* [2002] for a review of Mohr circles). (b) Illustration of components of the principal effective stresses and their ratio R', as a function of depth. Deviatoric stresses (compression positive) are added to the total isotropic pressure p_0 (hydrostatic plus hydrodynamic) and water pressure is subtracted. The resulting effective stress ratio varies with depth and can result in satisfaction of the slip criterion (gray-shaded area) near the surface.

compressive principal stress. The same subscripting convention is used for strain rates. If a body of ice is loaded such that the most compressive stress and strain rate are larger than the critical values indicated in equations (2) and (3), respectively, the ice should undergo macroscopic brittle faulting. This scheme for defining the onset of brittle fracture in ice is broadly consistent with a wide range of laboratory data [*Renshaw and Schulson*, 2001]. If the least compressive principal stress is tensile, the frictional terms disappear and the criterion for fracture can be expressed as [*Ashby and Hallam*, 1986]

$$\sigma_f = \frac{K_{Ic}}{\sqrt{\pi c}}. \tag{4}$$

The variables n, K_{Ic}, α, μ, and c in equations (2)–(4) are all properties of the ice that can be measured or estimated independently. The viscosity parameter B is temperature dependent, but for an isothermal glacier, it is considered constant. Therefore, the only independent variable is the stress ratio R, which may vary substantially in a glacier.

[12] If a fracture already exists that spans the thickness of the glacier and can be reactivated, as envisioned by *Hambrey et al.* [1999], only Coulomb friction resists fault motion, potentially mediated by the pressure of water that may fill the fracture. Retaining the principal stress notation, reactivation of such a fracture oriented at an angle θ to σ_1 can occur when [*Scholz*, 2002, equation (3.3)]

$$\frac{(\sigma_1 - p_w)}{(\sigma_3 - p_w)} = \frac{(1 + \mu \cot \theta)}{(1 - \mu \tan \theta)}, \tag{5}$$

where p_w is water pressure. Figure 3a illustrates a stress field that satisfies the Coulomb criterion on a fracture oriented at the optimal angle θ_o to the most compressive stress and with an arbitrary choice of p_w. This optimal orientation is a function of the friction angle ϕ,

$$\theta_o = \frac{\pi}{4} - \frac{\phi}{2}, \tag{6}$$

where $\phi = \tan^{-1}\mu$. In the absence of a fracture so oriented, slip would continue to be suppressed until either the applied stress increased or increased water pressure lowered the effective stresses sufficiently to cause movement. Figure 3b schematically illustrates the components of a hypothetical stress field that does not satisfy the Coulomb criterion across an entire fracture surface. In this example, water

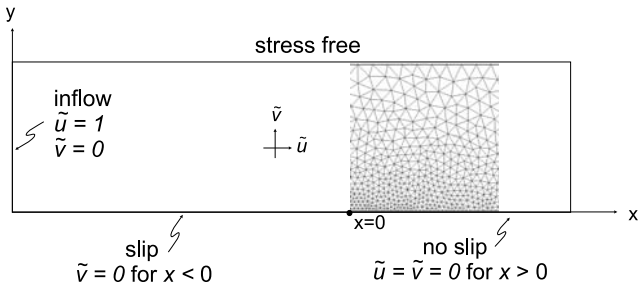

Figure 4. Generalized model domain, boundary conditions, and a representative portion of the numerical mesh.

pressure reduces friction in the lower 60% of the fracture, but the upper portion of the fracture remains dry. Nevertheless, because ice overburden pressure approaches zero near the surface while deviatoric stresses remain finite, the slip criterion is more readily satisfied near the surface, even under dry conditions.

[13] In both the fracture and slip criteria above, the stress fields are the primary independent variables. This allows both criteria to be readily evaluated everywhere in a glacier where the stress field can be determined, provided that material properties can be estimated.

3. Methods

[14] We use a 2-D finite element model of ice flow over a basal slip/no-slip transition (SNST) to evaluate whether thrust faulting is likely. The approach is to apply velocity boundary conditions at the inflow and the bed, and stress-free conditions on the surface, and then solve for englacial velocity and pressure fields assuming that the ice is macroscopically homogeneous and that all strain is accommodated by continuum viscous flow. Strain rates, and hence, stresses, are then determined from velocity gradients, and the fracture criteria are evaluated everywhere in the domain. Finally, we determine a posteriori whether the developed stresses and strain rates are sufficient to induce fracture or fault slip. No attempt is made to model the evolution of a fault once it has begun to propagate. Instead, the goal is to constrain the range of parameter space under which faulting can be initiated. The results are expected to be qualitatively relevant where ice undergoes longitudinal compression resulting from abrupt changes in basal drag, but can also be applicable where compressive stress regimes arise under different circumstances.

[15] The finite element method was implemented with ELMER, a public-license fluid dynamics package developed by the Finnish Center for Scientific Computing [*Gagliardini et al.*, 2007; *Gagliardini and Zwinger*, 2008]. The model domain was discretized using GMSH, which is also a public-license software. To retain generality, the model domain was a rectangular region with height equal to one and with length expressed in ice thicknesses. The length of the sliding portion of the glacier inside the domain affects velocity gradients away from the SNST, so this length l_0 is reported as $l_0 = kh_0$, where k is an integer constant. Flow is driven by velocity boundary conditions at the inlet and the bed, as illustrated in Figure 4, where dimensionless horizontal and vertical velocities are u_0 and v_0, respectively. The natural boundary condition at the upper surface is stress-free. As a consequence, ice can flow out of the domain across the upper boundary, as well as the right-hand boundary. This domain represents a segment of the lower ablation zone of a glacier that is driven by a constant ice flux from higher upglacier. This upper boundary condition differs from some past treatments of this problem in which no flow across the upper boundary was permitted, resulting in an acceleration of near-surface ice as it crossed the SNST [e.g., *Hutter and Olunloyo*, 1980; *Lliboutry*, 2002]. We are considering ice in the ablation zone of a glacier, so it is essential to permit ice flow (and therefore, discharge, which should be balanced by ablation) across the top. The significance of this issue is addressed in more detail in a separate paper [*Moore et al.*, 2009].

[16] In model simulations, we invoke an abrupt free-slip to no-slip transition at the bed, even though this may not be the most realistic portrayal of this transition in a glacier. Under such basal conditions, shear stress along the slipping portion of the bed must be zero and mass conservation controls how basal sliding velocity changes when it approaches the SNST. *Moore et al.* [2009] showed that basal slip velocity under these boundary conditions declines almost linearly from the inlet to the SNST, only becoming noticeably steeper within one half of an ice thickness from the SNST. The resultant longitudinal velocity gradients should be viewed as maxima, since both the implied no-drag sliding upglacier of the transition and the abrupt transition to no-slip are idealizations. Stresses are directly related to velocity gradients, so our simulations can be viewed as providing upper bounds for the stresses developed in such flows.

[17] According to analytical models of similar problems [e.g., *Hutter and Olunloyo*, 1980; *Lliboutry*, 2002], the slip/no-slip transition produces a stress singularity at the point of transition, such that stresses in the ice are infinite. Singularities like this are mathematical artifacts that cannot be manifested in nature. Numerical discretization is a means of smoothing out the singularity while still capturing the physics over length scales for which the continuum approximation is valid. Therefore, model meshes are refined near the slip transition, but only so that the edge length of the smallest elements is comparable to several crystal diameters when the domain is scaled [see *Moore et al.*, 2009].

[18] The model-governing equations are the nondimensional form of the Navier-Stokes equations, expressed for the power law case with inertia neglected:

$$\begin{aligned} &-\tilde{\nabla}\tilde{P} + \tilde{\nabla}\cdot\left[\tilde{\dot{\varepsilon}}_e^{(1-n/n)}\left(\tilde{\nabla}\tilde{\boldsymbol{v}} + \left(\tilde{\nabla}\tilde{\boldsymbol{v}}\right)^{\mathrm{T}}\right)\right] = 0, \\ &\tilde{\nabla}\cdot\tilde{\boldsymbol{v}} = 0, \end{aligned} \tag{7}$$

where P is the pressure deviation from hydrostatic and tildes ($\sim$) indicate nondimensional quantities. Gradients of the output velocities are used to determine the components of the dimensionless strain rate tensor, and corresponding components of the deviatoric stress tensor were computed with the relation

$$\tilde{\tau}_{ij} = \tilde{B}\tilde{\dot{\varepsilon}}_e^{(1-n/n)}\tilde{\dot{\varepsilon}}_{ij}. \tag{8}$$

Table 1. Parameter Values Used in Model Simulations

Parameter	Values	References[a]
B	9.0–10,000 MPa $s^{1/n}$	1
c	$\begin{cases} 0.002-0.005 \text{ m (Storglaciaren)} \\ 0.005-0.05 \text{ m (Variegated Glacier)} \end{cases}$	7 2
h_0	20–40 m	4
K_{Ic}	0.05–0.15 MPa $m^{1/2}$	3
l_0	4 h_0–13 h_0	4
n	1.0–4.2	4
v_0	$\begin{cases} 4.76 \times 10^{-7} \text{ ms}^{-1} \text{ (Storglaciaren)} \\ 2.0 \times 10^{-4} \text{ ms}^{-1} \text{ (Variegated Glacier)} \end{cases}$	4
α	1.0	5
μ	$\begin{cases} 0.1-1.0\text{(ice)} \\ 0.4-0.7\text{(debris)} \end{cases}$	6, 8
λ	0–0.915	–

[a]References: 1, *Cohen* [2000]; 2, *Pfeffer* [1992]; 3, *Fischer et al.* [1995]; 4, *Raymond et al.* [1987]; 5, *Renshaw and Schulson* [2001]; 6, *Schulson* [2001]; 7, *Paterson* [1994]; 8, *Maeno and Arakawa* [2004].

For subsequent manipulation, nodal values of velocity, pressure, deviatoric stresses, and strain rates are interpolated from the unstructured finite element grid onto a regular grid with the same minimum spacing. Use of principal stress ratios in the faulting criteria requires that fully scaled total stresses be used, so that each of the stress components is rescaled according to the boundary conditions and geometry of the model for each case studied. Therefore, total dimensional stresses are

$$\boldsymbol{\sigma} = \frac{B}{2}\left(\frac{u_0}{h_0}\right)^{1/n}\left(\tilde{P}\mathbf{I} - \tilde{\boldsymbol{\tau}}\right) + \rho_i g d\mathbf{I}, \tag{9}$$

where u_0 is the dimensional inflow velocity, $\mathbf{I}$ is the identity matrix, and d is the dimensional depth below the ice surface, with the ice thickness equal to h_0. Principal stresses and their orientations are computed with the standard relations

$$\sigma_{1,3} = \frac{1}{2}\left(\sigma_{xx} + \sigma_{yy}\right) \pm \left[\frac{1}{2}\left(\sigma_{xx} - \sigma_{yy}\right)^2 + \sigma_{xy}^2\right]^{1/2}, \tag{10}$$

$$\gamma = \frac{1}{2}\tan^{-1}\left(\frac{2\sigma_{xy}}{\sigma_{xx} - \sigma_{yy}}\right), \tag{11}$$

where γ is the angle between the x axis in the model coordinate system and σ_1. Strain rates substituted for stresses in these equations suffices for determining principal strain rates.

[19] To evaluate the fracture criteria, the value of R is determined at each node using the nodal principal stresses. When $R > 0$ is satisfied, both of the principal stresses are compressive, and equations (2) and (3) are evaluated to find the unique failure stress σ_f and brittle-ductile transition strain rate $\dot{\varepsilon}_{B/D}$ at each node. Incipient cracks are assumed to be isolated from interaction with water, so water pressure, therefore, has no role in fracture initiation (although water's impact on crack friction may be incorporated through its effect on the friction coefficient). The most compressive principal stress and strain rates at each node are then compared with these critical values. For ease of graphical representation in this and subsequent analyses of faulting criteria, the nodal values of maximum and critical stresses (and strain rates) are compared as ratios $R_\sigma \equiv \sigma_1/\sigma_f$, ($R_\varepsilon \equiv \dot{\varepsilon}_1/\dot{\varepsilon}_{B/D}$). Thus, a value of this ratio equal to or greater than 1 implies satisfaction of the stress (strain rate) criterion there. If $R < 0$, nodal values of σ_3 are compared with the tensile failure stress determined from the tensile fracture criterion (equation (4)) [*Ashby and Hallam*, 1986]. Where the relevant stress or strain rate equals or exceeds the critical value determined from a fracture criterion at multiple nodes (i.e., $R_\sigma \geq 1$ or $R_\varepsilon \geq 1$), initiation of brittle fracture is expected. Requiring satisfaction at multiple nodes further ensures that singularities do not affect the results. Since growth of a crack under steady stress generally results in enhanced stress concentrations at the crack tips, after initiation, a macroscopic crack is assumed to grow rapidly into a large fracture. Values of the material properties used to evaluate equations (3)–(5) are chosen from the literature as best estimates, and reasonable variations around these estimates are investigated to evaluate model sensitivity (Table 1).

[20] The Coulomb slip criterion is treated in a similar manner. The left-hand side of equation (5) is defined as the effective stress ratio R':

$$R' = \frac{(\sigma_3 - p_w)}{(\sigma_1 - p_w)}, \tag{12}$$

and the right-hand side of equation (5) is defined as the critical effective stress ratio:

$$R'_c = \frac{(1 - \mu\tan\theta)}{(1 + \mu\cot\theta)}. \tag{13}$$

Water pressure is scaled with the ice thickness by the parameter $\lambda = (\rho_w g h_w)/(\rho_w g h_0)$, such that $\lambda = \rho_i/\rho_w$ corresponds to water pressure equal to ice overburden, where ρ_w and ρ_i are the density of water and ice, respectively, and h_w is the height of the water table or potentiometric surface in the ice. Equation (13) is first solved at each node to define the critical effective stress ratio. The nodal principal stresses are then used in equation (12), and the ratio R'_c/R' is evaluated (this ratio is the reciprocal of the form used in the fracture criterion because the slip condition is approached as R' decreases). The preexisting fracture is first assumed to be optimally oriented everywhere. Water pressure is also first assumed to be zero, then increased until the criterion is satisfied. The same process is repeated for a family of nonoptimal fracture orientations. The friction coefficient used for the sliding interface is 0.5, a value that is reasonable for both granular materials and cold ice at low slip rates [*Lambe and Whitman*, 1969; *Kennedy et al.*, 2000], but it is varied through a large range (Table 1) to allow for different characteristics of the sliding interface.

[21] Several scenarios are considered, all of which involve 2-D flow through rectangular domains containing a basal SNST. In particular, domain characteristics for two groups of simulations are chosen to roughly approximate stress fields in two contrasting cases: (1) the terminus of Variegated Glacier in 1983 where a surge front propagated into stagnant ice and (2) the temperate-based to cold-based transition (basal thermal transition or BTT) at the margin

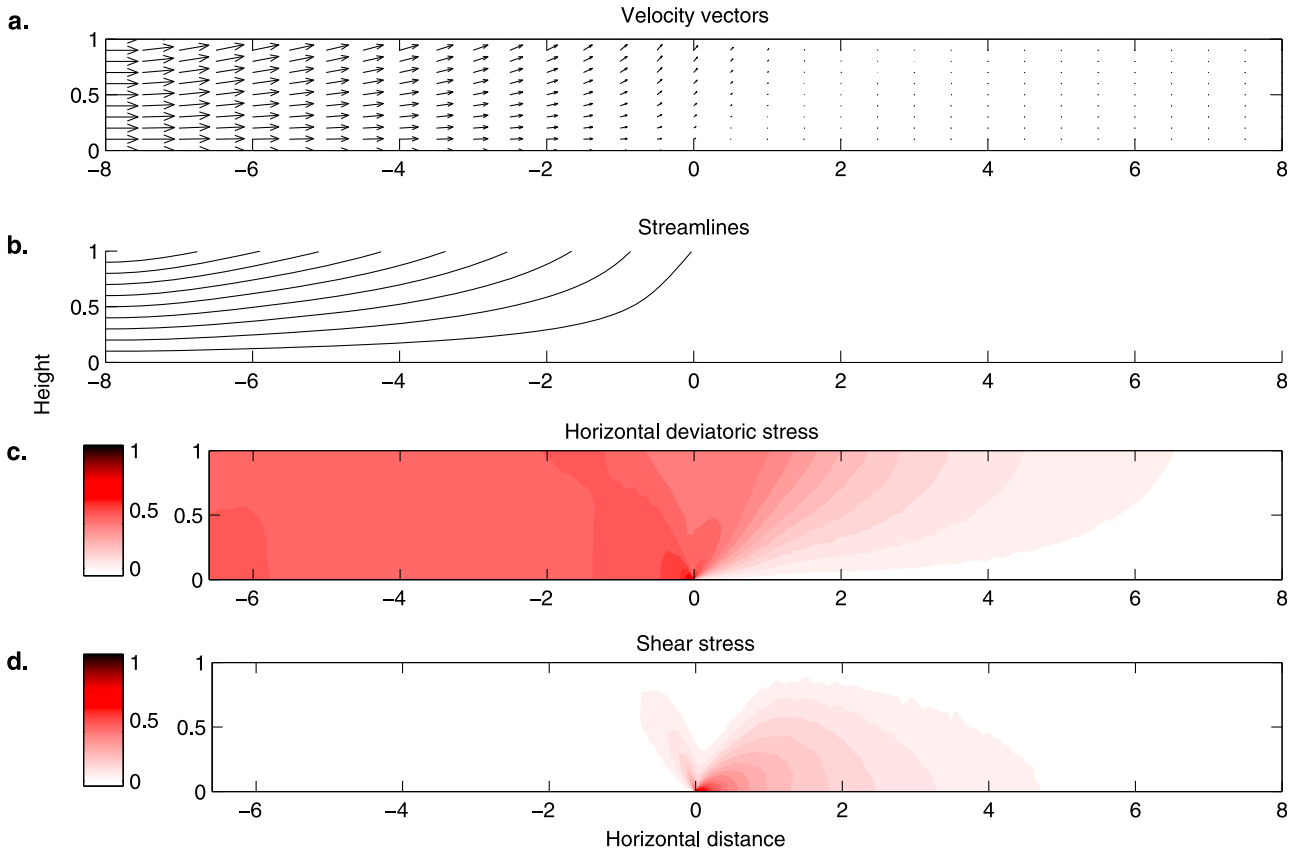

Figure 5. Sample dimensionless velocity and stress results from a simulation with $l_0 = 8h_0$ and $n = 3$. (a) Velocity vectors. (b) Steady state streamlines. (c) Longitudinal deviatoric stress. (d) Shear stress.

of a polythermal glacier such as Storglaciären. While the Variegated surge termination did not coincide with a BTT, the SNST, where the surge propagated into stagnant marginal ice, is mechanically similar to a BTT. Information for the Variegated Glacier case is drawn from literature [*Kamb et al.*, 1985; *Raymond et al.*, 1987; *Sharp et al.*, 1988; *Pfeffer*, 1987, 1992], while frozen margin parameters are derived from field data obtained from ongoing research at Storglaciären [*Moore et al.*, 2008] as well as from *Jansson et al.* [2000].

4. Results

[22] Nondimensional velocity and deviatoric stress fields for all of our finite element simulations are qualitatively similar. Values of n affect these fields in only subtle ways. Figure 5 shows an example of the velocity and deviatoric stress solutions for a domain with a sliding length $l_0 = 8h_0$ and $n = 3$. The transition from free-slip to no-slip boundary conditions is at $x = 0$, resulting in longitudinal compression and vertical extension in the ice approaching the SNST. Horizontal deviatoric stresses are nearly uniform beyond 1.5 ice thicknesses upstream of the SNST. Basal shear stress, required by the boundary conditions to be zero in the sliding portion of the bed, peaks at the SNST and returns to negligible values beyond two ice thicknesses downstream.

[23] Dimensional total stress magnitudes and orientations are strongly affected by a SNST, as illustrated in Figure 6. The principal stress ratio (R), shown in Figure 6, reaches a maximum value ($R = 1.0$) on the right-hand side of the domain where deviatoric stresses become small and the stress field is nearly hydrostatic. Upstream of the SNST, deviatoric stress magnitudes are nonnegligible, and can be quantified with equation (9), and dimensional variables B, h_0, and u_0. The stress field in Figure 6 corresponds to $B = 77$ MPa $s^{1/3}$, $h_0 = 25$ m, and $u_0 = 4.8 \times 10^{-7}$ m s^{-1}, values roughly appropriate for the terminus region of Storglaciären. The associated principal stress ratio R and the related effective stress ratio R' are the primary variables determining whether either fracture or slip occurs. Except near the SNST, the deviatoric stresses are independent of depth, as shown in Figure 5c. However, the hydrostatic component of the total stress field is a function of depth and becomes a smaller fraction of the total stress field near the surface. As a consequence, the principal stress ratio (i.e., the degree of confinement) decreases upward even though the deviatoric stress does not (Figure 6).

4.1. Fracture Criteria

[24] Figure 7 shows the results when the fracture criteria (equations (2) and (3)) are evaluated for the stress field shown in Figure 6, appropriate for conditions at Storglaciären. The strain rate criterion is satisfied when $R_\varepsilon = \dot{\varepsilon}_1/\dot{\varepsilon}_{B/D} \geq 1$, and likewise, the stress criterion is satisfied if $R_\sigma = \sigma_1/\sigma_f \geq 1$. Each ratio reaches a peak value in a small region around the SNST. However, values are approximately five and one

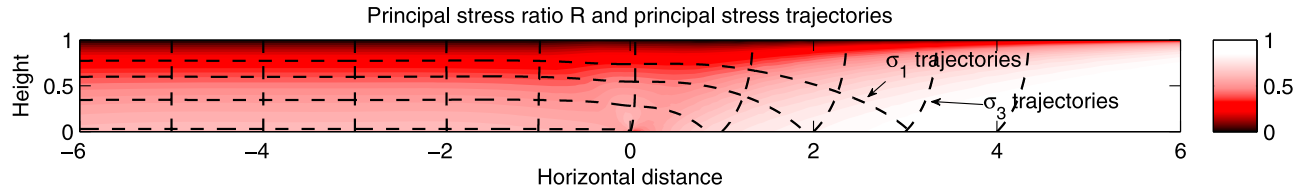

Figure 6. Principal stress ratio R and principal stress trajectories for the same simulation shown in Figure 5.

orders of magnitude too small for the strain rate and stress criteria, respectively, so neither criterion is satisfied. In all simulations, the stress criterion is closer to being achieved than the strain rate criterion. Since both components must be satisfied to accomplish fracture, we hereafter focus on results with only the strain rate criterion.

[25] Evaluation of the strain rate criterion for the Variegated surge-front simulations is shown in Figure 8. In this simulation, $l_0 = 13h_0$, $h_0 = 25$ m, $u_0 = 2.38 \times 10^{-4}$ m s^{-1}, $n = 4.2$, and $B = 9$ MPa s$^{1/4.2}$ (Table 1). In Figure 8 (left), only the compressive fracture criterion is evaluated, and the numerical values of R_ε near the SNST are no more than about 10^{-3}. Just downstream from the SNST is an area where deviatoric stresses are elevated sufficiently so that the least compressive deviatoric stress (plunging steeply upglacier in this region, as in the case illustrated by σ_3 in Figure 6) is larger in magnitude than the weight of the overlying ice, making the least compressive principal stress negative or tensile. There, the frictional components of the fracture criterion vanish, and the conditions for fracture can be described by equation (4). In Figure 8 (right), the area around this tensile regime is enlarged, and the tensile criterion is evaluated, reaching values much closer to, but still less than 1.

[26] Given that many of the input parameters in the fracture criterion are poorly constrained for Variegated Glacier, we consider the effects on R_ε of varying several of these parameters, including the viscosity parameter B, fracture toughness K_{Ic}, inflow velocity u_0, crack length c, and crack-surface friction coefficient μ. The results are shown in Figure 9, where one parameter at a time is varied through a reasonable range (see Table 1). In all cases, parameter adjustments that tended to increase R_ε also caused the value of σ_3 to become negative, indicating that fracture would proceed only in tension. Nevertheless, reasonable variations of B and inflow velocity were all capable of satisfying the tensile fracture criterion in a small region (comprising several nodes) just downglacier from the SNST.

4.2. Frictional Slip Criteria

[27] The Coulomb slip criterion is evaluated for the same simulations described in the fracture analysis. Where there is a preexisting, penetrative fracture that is isolated from interaction with water, the stress field is unchanged from the equivalent fracture-criterion case. The stress field under these circumstances is the same as that shown in Figure 6. The optimal slip plane (which is not generally the orientation of maximum shear stress [*Scholz*, 2002]) is at some angle θ_0, given in equation (6), to the most compressive principal stress shown in Figure 6. Slip will be most likely along fractures at this orientation. Figure 10a shows the Coulomb slip criterion evaluated for this stress field with $\mu = 0.5$, appropriate for a fracture filled with ice-free debris. Orientations of optimal slip surfaces (dashes) are also shown. Very near the top of the domain and upglacier of the SNST in this simulation, where there is finite longitudinal compression, but very little overburden stress, the criterion is satisfied. Everywhere below this near-surface horizon, and therefore, along the plane of any bed-intersecting fracture, the criterion is not satisfied. Therefore, slip extending to the bed is not expected under dry conditions with $\mu = 0.5$. However, for the stress field corresponding to

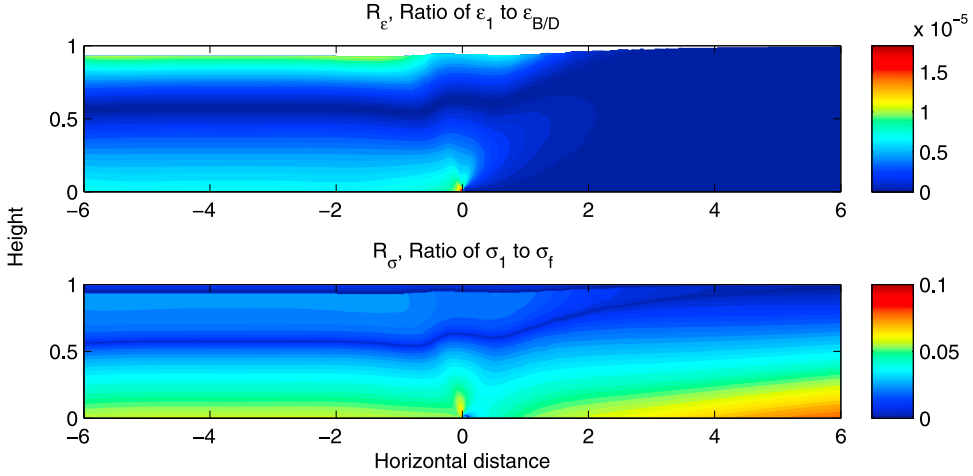

Figure 7. Evaluation of compressive fracture criterion for the simulation shown in Figures 5 and 6, representing Storglaciaren's frozen margin. (top) Strain rate criterion. (bottom) Stress criterion.

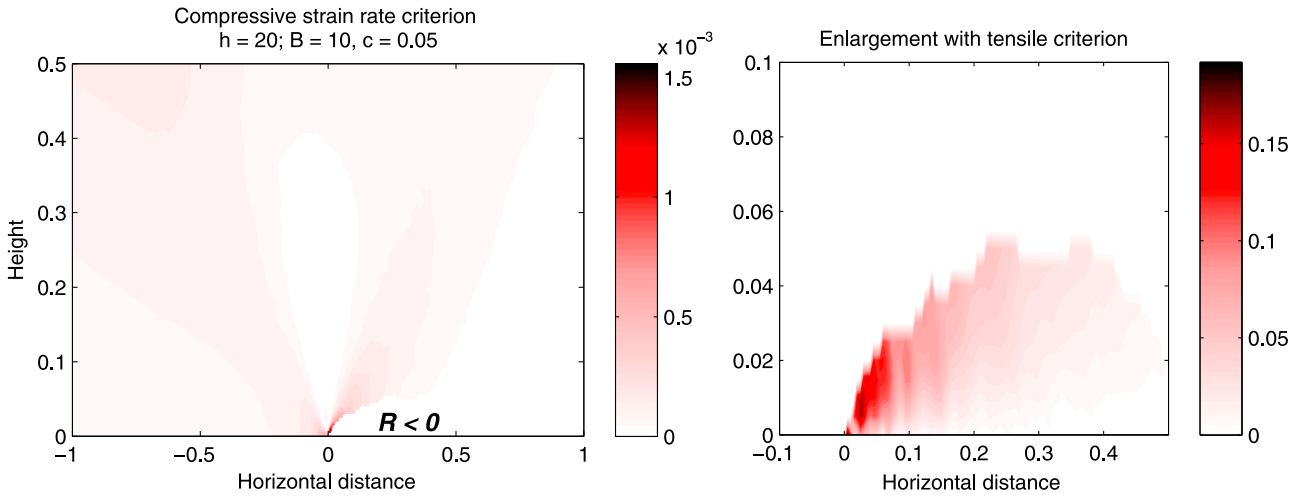

Figure 8. Evaluation of strain rate criterion for simulation representing the surge front at the 1983 termination of the Variegated Glacier surge. (left) Compressive strain rate criterion only. A small zone between $x = 0$ and $x = 0.5$, and below about $y = 0.05$ is subject to tensile stress. (right) Enlargement of the tensile stress zone with both the compressive and tensile fracture criterion evaluated.

the Variegated surge front, slip on optimally oriented fractures could readily occur over a large area upglacier from the SNST under dry conditions (Figure 10b).

[28] If water is permitted to fill the preexisting fracture to a certain height under hydrostatic pressure commensurate with that height, frictional resistance to slip is expected to decline according to equation (5), and wholesale slip should

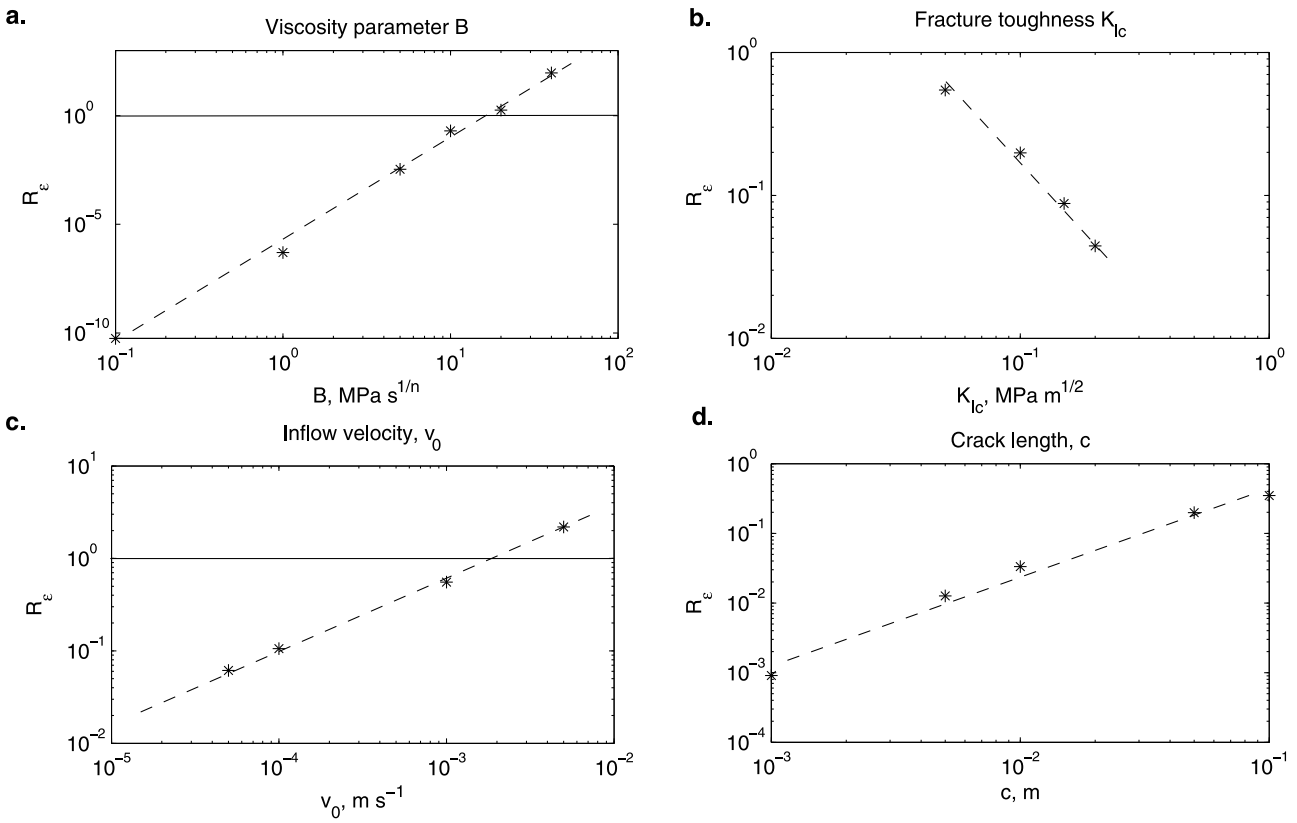

Figure 9. Model sensitivity to input parameters for the Variegated simulation shown in Figure 8. For each plot, one parameter is varied while all other parameters are held constant at the "best guess" values taken from the literature, and the strain rate criterion is reevaluated. (a) Variation of viscosity parameter B. (b) Variation of ice fracture toughness K_{Ic}. (c) Variation of inflow velocity u_0 in m s^{-1}. (d) Variation in crack length c, corresponding to half of the crystal diameter.

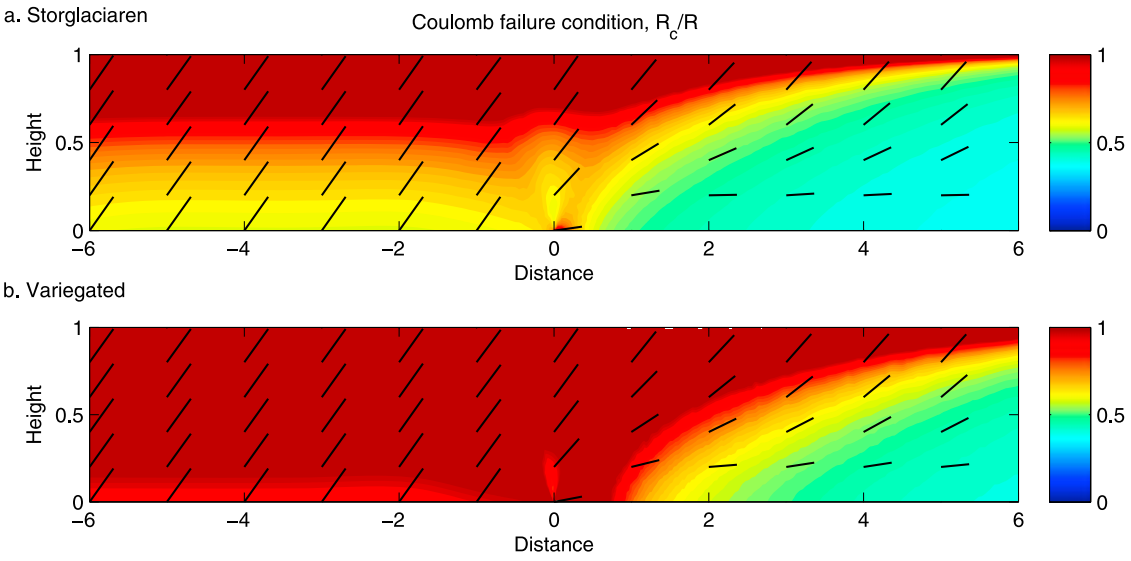

Figure 10. Evaluation of the Coulomb slip criterion with no water pressure on an englacial sliding interface for (a) a simulation representing Storglaciaren's frozen margin and (b) a simulation representing the surge termination at Variegated Glacier. Hachures are parallel to the "optimal" fracture orientation θ_0. The ratio R_c/R is inverted compared to the fracture criterion because slip occurs if $R \leq R_c$.

become more feasible. For the stress field illustrated in Figure 10, an increase in water pressure up to 80% of the ice thickness ($\lambda = 0.8$) results in satisfaction of the slip criterion through nearly the entire thickness of the glacier within two ice thicknesses of the SNST, as shown in Figure 11a. If on an optimally oriented fracture through this zone, there are small patches where the criterion is not satisfied (Figure 11b), stress concentrations there will likely cause slippage over the entire fracture surface [cf. *Palmer and Rice*, 1973]. In any case, further increasing the water pressure in the same fracture closer to ice overburden pressure permits complete satisfaction of the slip criterion along an optimal surface.

[29] If no fractures are optimally oriented, the picture changes significantly. For the case above, where the criterion is almost fully satisfied for the length of a penetrative fracture when water pressure is close to ice overburden pressure, a fracture that is rotated by 10° from the optimum is far from satisfying the criterion. Figure 11c shows the effect of rotation of the preexisting fracture by 10° and 20° in either direction from optimum. In any orientation outside of about a 5° window around the optimum, water pressure must reach ice overburden pressure before the fracture will be permitted to slip for $\mu = 0.5$. This result, however, is sensitive to the value of μ. As shown in Figure 11d, raising μ above 0.5 reduces the probability of slip, whereas lowering μ greatly broadens the range of water pressures for which slip is permitted.

5. Discussion

[30] The model results presented here indicate that the compressive fracture criterion for ice in the work of *Renshaw and Schulson* [2001] and *Schulson* [2001] is not satisfied for any reasonable combinations of the input parameters used. The simple interpretation of this result is that even under exceptional glaciological circumstances, creation of a thrust fault by compressive fracture of initially homogeneous ice will not be possible. However, under extreme circumstances, it may be possible to induce tensile fracture if the least compressive principal stress becomes negative. The results also show that given an optimally oriented, penetrative fracture subjected to large compressive stresses, slip may occur under limited conditions.

[31] Glaciers are not likely to be totally homogeneous as we have assumed in evaluating the fracture criterion, nor are they likely to have many existing fractures that both penetrate the full thickness and width of the glacier, and are optimally oriented. Much more likely are a large number of preexisting, variously oriented, macroscopic flaws that extend for distances on the order of 10^{-3} to 10^{-1} ice thicknesses [e.g., *Fountain et al.*, 2005]. These fractures may terminate in unfractured ice at depth and at their lateral extent so that even if slip at some point in the center of the fracture is resisted only by Coulomb friction along the fracture interface, there will be additional viscous resistance offered by ice above and below the ends of the fracture. Under these circumstances, neither the fracture model nor the Coulomb slip model, as presented above, is strictly applicable, but they nevertheless represent upper and lower bounds for the behavior of intermediate cases. For example, a crevasse trace that spans only 25% of the ice thickness and is not optimally oriented should resist slip more than an equivalent fully penetrating crevasse. Frictional resistance must be overcome to initiate slip on such a crevasse trace, but even when this condition has been met, thrusting involving the full ice thickness requires propagation of the crevasse trace to the bed by fracture. On the other hand, such a crevasse trace, because of its size (i.e., consider the effect of increasing the value of crack half-length c in equations (2) and (3)), will grow under a less compressive stress field than grain-scale flaws in a macroscopically homogeneous glacier. In other words, where preexisting fractures are present but do not penetrate the full ice thickness, thrusting should be favored under a more limited range

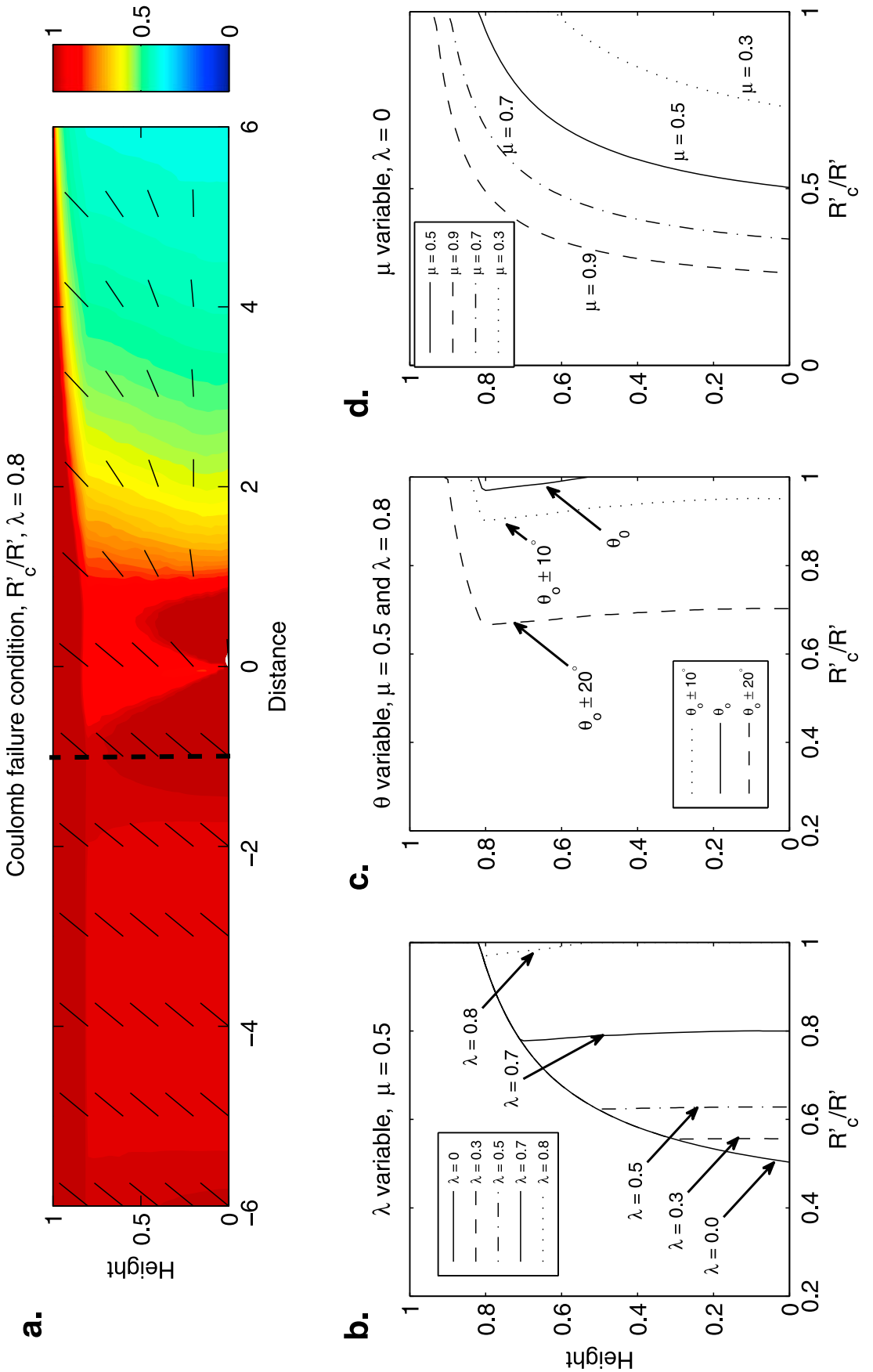

Figure 11. Evaluation of the Coulomb criterion for the Storglaciären simulation and variation about best-guess values of parameters. (a) Hydraulic head equal to 0.8 times the ice thickness. (b–d) Along-fracture profiles of the Coulomb criterion near the vertical dashed line in Figure 11a. Variation of water pressure is shown in Figure 11b. Variation of fracture orientation about the optimum is shown in Figure 11c. Variation of friction coefficient is shown in Figure 11d.

of conditions (e.g., orientation closer to optimal, higher water pressures, and weaker slip surface) than those that would permit slip on a fully penetrative fracture.

5.1. Frozen-Margin Simulations

[32] Longitudinal strain rates across BTTs in nonsurging polythermal glaciers like Storglaciären are orders of magnitude smaller than those in surge fronts. In such situations, thrusting must be preceded by the development of a large preexisting fracture with an orientation that is near optimum. The fracture criterion does not predict compressive fracture with any reasonable variation of model parameters in simulations representing the frozen margin of Storglaciären (Figure 7). Results for preexisting fractures indicate that slip will occur only if the fracture orientation is near optimal and hydrostatic water pressures within the fracture are close to ice overburden pressure (Figure 11b). Upward seepage of water through a permeable fracture would further promote slip because of water pressures in excess of hydrostatic necessary to drive water flow.

5.2. Variegated Glacier Simulations

[33] Simulations with conditions appropriate for Variegated Glacier were driven with large far-field compressive strain rates u_0/l_0h_0, but the computed peak compressive strain rates near the SNST were too small to exceed the rate at which ice creep around incipient crack tips could accommodate strain. Instead, under such intense longitudinal compression, a region near the SNST was subject to net tensile stress. This tensile stress results from the least compressive deviatoric stress being larger than (and of opposite sign as) the isotropic component of the stress tensor. With some reasonable combinations of material parameters, the tensile failure criterion could be satisfied in this zone (Figures 9a and 9c). A tensile fracture in this area would open parallel to and extend normal to the tensile stress vector, which dips in the upglacier direction (Figure 6), producing a downglacier dipping fracture: the opposite orientation of that expected for a thrust fault. While downglacier-dipping tensile fractures alone cannot explain the mechanism of thrusting at the Variegated surge termination, the tensile stress regime may have promoted initial crack opening and buckling of ice. Indeed, *Sharp et al.* [1988] describe the appearance of thrust faults at the surface of Variegated Glacier only after a period of folding and buckling of surface ice. Model results of *Pfeffer* [1987] show the development of zones of tensile stress near the surge front. Pfeffer further suggests that thrust faulting could develop in these zones as a result of hydrofracturing: growth of an array of tensile cracks, with the mechanical assistance of pressurized water. Growth and linkage of such fractures could provide a zone of damaged ice sufficient to eventually allow thrusting along upglacier-dipping surfaces.

[34] An alternative possibility is that preexisting fractures were reactivated during the surge. Model results indicate that any penetrative fracture that was reasonably close to the optimal orientation would slip readily even under low water pressures (Figure 10). Since basal water pressures were known to be remarkably high during the Variegated surge, even penetrative fractures that were not oriented near the optimum could potentially have been activated. However, no such reactivated fractures have been documented. On the contrary, *Pfeffer* [1987] identified several upglacier-dipping, sediment-filled structures near the lower extent of surging that presumably existed prior to the 1982–1983 surge and found no evidence that they accommodated slip during the surge.

5.3. Other Considerations

[35] We have, thus far, neglected any cohesion (unconfined strength) of preexisting fractures. This may indeed be an appropriate assumption for fracture planes that are filled with grain-supported sediment. However, cohesion increases as a function of volumetric ice content for frozen granular materials and the cohesive term in the full Coulomb equation follows Glen's law [*Arenson and Springman*, 2005]. Consideration of this case is beyond the scope of this paper, but nevertheless, it indicates that any ice-supported debris-rich structures in ice will resist shearing more than the cohesionless model presented here.

[36] A notable and pervasive feature of the Coulomb simulations is a near-surface zone of slip, even in the absence of water (Figures 10 and 11). This is a result of the nonzero horizontal deviatoric stresses where ice overburden pressure becomes zero at the glacier surface. Thus, if the longitudinal compression is sustained, slow slip on preexisting cracks could occur near the surface and be accommodated by flow at depth. This could give the appearance of fault offset at the ice surface even if the active portion of the fault did not extend more than a few meters deep. Similar features have been described on numerous glaciers [e.g., *Weertman*, 1961, and references therein; *Rabus and Echelmeyer*, 1997], although efforts to document slip on them have generally not been successful. The lack of evidence for discrete displacements across such features has led some authors to suggest that the surface relief often seen across thin debris layers is a result of differential ablation [e.g., *Hooke*, 1973].

[37] If a preexisting fracture is not filled with sediment, the mechanical behavior of the interface under a compressive stress field is incompletely known. In the absence of debris and pressurized interfacial water, sintering could become important. Laboratory experiments have demonstrated that sintering strengthens an ice-ice interface because plastic flow around asperities allows an increase in real contact area, enhanced by large normal forces and high homologous temperatures [e.g., *Szabo and Schneebeli*, 2007]. In laboratory experiments, *Maeno and Arakawa* [2004] showed that even ice surfaces slipping across one another at small displacement rates (10^{-6}–10^{-8} m s^{-1}) experienced transient sintering that increased with temperature. For example, at a temperature of -5°C and a sliding rate of 10^{-8} m s^{-1} (reasonable values for a hypothetical sliding fracture in Storglaciären's terminus), a model based on their data predicts that an ice-ice sliding interface is nine times stronger than the same interface sliding at 10^{-4} m s^{-1}, and could exhibit friction coefficients in excess of 1.0. In the limit that sintering allows the real contact area to equal the entire area of the interface, there is no fracture and the ice should behave as a continuum [cf. *Maeno and Arakawa*, 2004]. The consequences of sintering in the present context are that a preexisting fracture surface, lacking debris, could heal in glacier ice subject either to normal compression or slow shear, resulting not only in a strengthened interface

but one sealed from interaction with water. In this case, sediment-filled structures would be favored for activation, and thrusting could not be invoked for incorporating sediment into the ice.

[38] Our steady state approach to modeling fracture and slip neglects the possibility that transients may be involved in fracture formation or propagation. Brief stress transients associated with reorganization of basal shear stress or basal water storage may be important means of fracture propagation. *Kavanaugh and Clarke* [2000] and *Kavanaugh* [2009] have shown that water in frozen-over boreholes in glaciers can very briefly (<1 s) reach pressures far exceeding ice overburden pressure. A likely cause for such events is local abrupt slip, causing longitudinal stress transfer in the ice. These longitudinal stresses compress or dilate the water-filled boreholes, suggesting that englacial stresses can vary considerably over short periods. The elevated water pressures further raise the possibility that pressure pulses might promote hydraulic fracture. Nevertheless, even if fracture is aided by these processes, subsequent slip is required to produce thrust offset and this slip must be governed by a slip criterion.

[39] The simulations presented here have been designed to err on the side of overestimating deviatoric stresses. By employing an abrupt SNST, we allow large stress concentrations to develop near the point of transition. Relaxing this constraint would reduce peak deviatoric stresses and strain rates, making them even smaller in comparison to critical values needed for fracture. The immediate neighborhood of the SNST is where R_ε is maximized, so smoothing the SNST would make fracture even less likely. This adjustment, however, would not necessarily inhibit Coulomb slip. Conditions favoring Coulomb slip on preexisting fractures are enhanced near the SNST but are also enhanced over a large portion of the glacier surface upglacier from the SNST.

[40] In summary, the conditions necessary to cause thrusting are probably uncommonly met in real glaciers. The primary variable that determines the critical field values of stress and strain rate is the stress ratio, which describes the degree of "confinement" (equations (2) and (3)). Where confinement is large, both fracture and slip are inhibited. For a given glacier with fixed material properties (i.e., B, n, c, K_{Ic}, μ, and α) the degree of confinement roughly scales with the ratio of the longitudinal velocity gradient to ice thickness. Greater longitudinal velocity gradients result in greater deviatoric stresses, but thicker ice increases confinement (equation (9)). Compressive fracture is, therefore, possible where compressive strain rates are large in thin ice, such as in drifting sea and lake ice. Frictional slip on preexisting fractures is also favored by these conditions, although it may be possible with reduced deviatoric stresses and thicker ice if the fractures are weakened by elevated water pressures approaching flotation. Indeed, elevated subglacial water pressures are common and can enable slip if the water can access the slip surface such as in a fracture containing porous sediment. Frictional slip, however, is inhibited if the fracture is strong (as might be the case if it has healed under normal compression), oriented oblique to the optimal angle defined by equation (6), or sealed from communication with water. Most glaciers are sufficiently thick so that the longitudinal velocity gradients they normally experience can be accommodated fully by ductile flow without ever surpassing the threshold for frictional slip or fracture. Exceptions are likely limited to surge fronts or glaciers with extensive preexisting fractures that already contain unfrozen water-saturated sediment and are inclined $30°-40°$ from the ice flow direction.

6. Conclusions

[41] Our results suggest that thrust faulting should be rare in glacier termini. A compressive fracture criterion for ice is not satisfied for the extreme case represented by the 1983 surge termination of Variegated Glacier. Instead, the thrusting observed there is more likely to have been the result of folding and tensile fracturing exacerbated by pressurized water, as envisioned by *Pfeffer* [1987], *Raymond et al.* [1987], and *Sharp et al.* [1988]. Nevertheless, thrusting cannot be precluded entirely if a preexisting fracture is present. Conditions permitting the development of thrust faults are: (1) thin ice subject to large horizontal compressive strain rates and (2) large, optimally oriented preexisting fractures in hydraulic communication with high-pressure water. The former condition points to thin glacier termini, particularly where they are influenced by surges. The latter condition favors structures already containing concentrated sediment, and therefore, requires that sediment be emplaced along the preexisting surface by some other process.

Notation

B	viscosity parameter in Glen's law, MPa $s^{1/n}$.
B^*	fluidity parameter in Glen's law, MPa^{-n} s^{-1}.
c	crack length, m.
d	depth below ice surface, m.
g	acceleration due to gravity, m s^{-2}.
h_0	ice thickness, m.
h_w	height of water table in fracture, m.
$\mathbf{I}$	identity matrix.
k	number of ice thicknesses in domain upstream of SNST.
K_{Ic}	fracture toughness of ice, MPa $m^{1/2}$.
l_0	length of domain upstream from SNST, $l_0 = kh_0$, m.
n	exponent in Glen's law.
p_w	water pressure, MPa.
$\tilde{P}$	dimensionless pressure deviation from hydrostatic.
R	confinement ratio $R = \sigma_3/\sigma_1$.
R_c	critical value of confinement ratio R for slip.
R'	effective confinement ratio $R = \sigma'_3/\sigma'_1$.
R'_c	critical value of effective confinement ratio R' for slip.
R_ε	strain rate criterion ratio $R_\varepsilon = \dot{\varepsilon}_1/\dot{\varepsilon}_{B/D}$.
R_σ	stress criterion ratio $R_\sigma = \sigma_1/\sigma_f$.
u	dimensionless horizontal velocity.
u_0	inflow velocity in x direction, m s^{-1}.
v	dimensionless vertical velocity.
$\tilde{\mathbf{v}}$	dimensionless velocity vector.
α	aspect ratio of columns bounded by wing cracks.
γ	angle between x axis and σ_1.
$\dot{\varepsilon}_e$	effective strain rate, $\dot{\varepsilon}_e = \sqrt{\frac{1}{2}\dot{\varepsilon}_{ij}\dot{\varepsilon}_{ij}}$, s^{-1}.
$\tilde{\dot{\varepsilon}}_e$	dimensionless effective strain rate.
$\dot{\varepsilon}_{ij}$	strain rate tensor components.
$\dot{\varepsilon}_{B/D}$	strain rate at brittle-ductile transition, s^{-1}.
θ	angle between fracture and σ_1.

θ_o optimal fracture angle.
λ water pressure parameter, $\lambda = h_w/h_0$.
μ friction coefficient.
ρ density, kg m^{-3}.
σ_1 most compressive principal stress, MPa.
σ_3 least compressive principal stress, MPa.
σ_f stress required for brittle failure, MPa.
σ_{xx} total stress in x direction, MPa.
σ_{yy} total stress in y direction, MPa.
σ_{xy} shear stress, MPa.
τ_e effective shear stress, $\tau_e = \sqrt{\frac{1}{2}\tau_{ij}\tau_{ij}}$, MPa.
τ_y Coulomb yield stress, MPa.
τ_{ij} deviatoric stress tensor components, MPa.
$\tilde{\boldsymbol{\tau}}$ dimensionless deviatoric stress tensor.
φ coefficient of internal friction.
$\tilde{\nabla}$ dimensionless gradient operator.

[42] **Acknowledgments.** The authors thank T. Rudolphi and E. Schulson for helpful discussions, J. Ruokolainen, T. Zwinger, and O. Gagliardini for assistance with model implementation, and R. Hooke, P. Hudleston, and N. Glasser for helpful comments on an earlier draft of this paper.

References

Alley, R. B., K. M. Cuffey, E. B. Evenson, J. C. Strasser, D. E. Lawson, and G. J. Larson (1997), How glaciers entrain and transport basal sediment: Physical constraints, *Quat. Sci. Rev.*, *16*, 1017–1038, doi:10.1016/S0277-3791(97)00034-6.

Arenson, L. U., and S. M. Springman (2005), Mathematical descriptions for the behavior of ice-rich frozen soils at temperatures close to 0°C, *Can. Geotech. J.*, *42*, 431–442, doi:10.1139/t04-109.

Ashby, M. F., and S. D. Hallam (1986), The failure of brittle solids containing small cracks under compressive stress states, *Acta Metall.*, *34*(3), 497–510, doi:10.1016/0001-6160(86)90086-6.

Bennett, M. R., D. Huddart, and R. I. Waller (2000), Glaciofluvial crevasse and conduit fills as indicators of supraglacial dewatering during a surge, Skeiðarárjokull, Iceland, *J. Glaciol.*, *46*, 25–34, doi:10.3189/172756500781833232.

Bishop, B. C. (1957), Shear moraines in the Thule area, northwest Greenland, *Res. Rep. 17*, U.S. Snow, Ice, and Permafrost Res. Estab., Wilmette, Ill.

Clarke, G. K. C., and E. W. Blake (1991), Geometric and thermal evolution of a surge-type glacier in its quiescent state: Trapridge Glacier, Yukon Territory, Canada, 1969–1989, *J. Glaciol.*, *37*, 158–169.

Cohen, D. (2000), Rheology of ice at the bed of Engabreen, *J. Glaciol.*, *46*(155), 611–621.

Ensminger, S. L., R. B. Alley, E. B. Evenson, D. E. Lawson, and G. J. Larson (2001), Basal crevasse-fill origin of laminated debris bands at Matanuska Glacier, Alaska, USA, *J. Glaciol.*, *47*, 412–422, doi:10.3189/172756501781832007.

Fischer, M. P., R. B. Alley, and T. Engelder (1995), Fracture toughness of ice and firn determined from a modified ring test, *J. Glaciol.*, *41*(138), 383–394.

Fountain, A. G., R. W. Jacobel, R. Schlichting, and P. Jansson (2005), Fractures as the main pathways of water flow in temperate glaciers, *Nature*, *433*, 618–621, doi:10.1038/nature03296.

Fowler, A. C., T. Murray, and F. S. L. Ng (2001), Thermally controlled glacier surging, *J. Glaciol.*, *47*, 527–538, doi:10.3189/172756501781831792.

Gagliardini, O., and T. Zwinger (2008), The ISMIP-HOM benchmark experiments performed using the finite-element code Elmer, *Cryosphere*, *2*(1), 67–76.

Gagliardini, O., D. Cohen, P. Raback, and T. Zwinger (2007), Finite-element modeling of subglacial cavities and related friction law, *J. Geophys. Res.*, *112*, F02027, doi:10.1029/2006JF000576.

Glasser, N., M. J. Hambrey, M. R. Bennett, and D. Huddart (2003a), Comment on Woodward et al., 2002, *J. Quat. Sci.*, *18*(1), 95–97, doi:10.1002/jqs.737.

Glasser, N. F., M. J. Hambrey, J. L. Etienne, P. Jansson, and R. Pettersson (2003b), The origin and significance of debris-charged ridges at the surface of Storglaciaren, northern Sweden, *Geogr. Ann., Ser. A*, *85*, 127–147, doi:10.1111/1468-0459.00194.

Goldthwait, R. P. (1951), Development of end moraines in east-central Baffin Island, *J. Glaciol.*, *59*, 567–577.

Hambrey, M. J., and F. Muller (1978), Structures and ice deformation in the White Glacier, Axel Heiberg Island, Northwest Territories, Canada, *J. Glaciol.*, *20*, 41–66.

Hambrey, M. J., J. A. Dowdeswell, T. Murray, and P. R. Porter (1996), Thrusting and debris entrainment in a surging glacier: Bakaninbreen, Svalbard, *Ann. Glaciol.*, *22*, 241–248.

Hambrey, M. J., D. Huddart, M. R. Bennett, and N. F. Glasser (1997), Genesis of "hummocky moraines" by thrusting in glacier ice: Evidence from Svalbard and Britain, *J. Geol. Soc. London*, *154*, 623–632, doi:10.1144/gsjgs.154.4.0623.

Hambrey, M. J., M. R. Bennett, J. A. Dowdeswell, N. F. Glasser, and D. Huddart (1999), Debris entrainment and transport in polythermal valley glaciers, *J. Glaciol.*, *45*, 69–86.

Herbst, P. F. N., and M. P. J. Schopfer (2006), The development of brittle structures in an alpine valley glacier: Pasterzenkees, Austria, 1887–1997, *J. Glaciol.*, *52*, 128–136, doi:10.3189/172756506781828872.

Hooke, R. L. (1973), Flow near the margin of the Barnes Ice Cap, and the development of ice-cored moraines, *Geol. Soc. Am. Bull.*, *84*, 3929–3948, doi:10.1130/0016-7606(1973)84<3929:FNTMOT>2.0.CO;2.

Hooke, R. L. (2005), *Principles of Glacier Mechanics*, 2nd ed., Cambridge Univ. Press, New York.

Hooke, R. L., and P. J. Hudleston (1978), Origin of foliation in glaciers, *J. Glaciol.*, *20*, 285–299.

Hutter, K., and V. O. S. Olunloyo (1980), On the distribution of stress and velocity in an ice strip, which is partly sliding over and partly adhering to its bed, by using a Newtonian viscous approximation, *Proc. R. Soc. London, Ser. A*, *373*, 385–403, doi:10.1098/rspa.1980.0155.

Jansson, P., J.-O. Naslund, R. Pettersson, C. Richardsson-Naslund, and P. Holmlund (2000), Debris entrainment and polythermal structure in the terminus of Storglaciaren, in *Debris-Covered Glaciers*, edited by M. Nakawo, C. F. Raymond, and A. Fountain, *IAHS Publ.*, *264*, 143–152.

Kamb, B., C. F. Raymond, W. D. Harrison, H. Engelhardt, K. A. Echelmeyer, N. Humphrey, M. M. Brugman, and T. Pfeffer (1985), Glacier surge mechanism: 1982–1983 surge of Variegated Glacier, Alaska, *Science*, *22*(4686), 469–479, doi:10.1126/science.227.4686.469.

Kavanaugh, J. L. (2009), Exploring glacier dynamics with subglacial water pressure pulses: Evidence for self-organized criticality?, *J. Geophys. Res.*, *114*, F01021, doi:10.1029/2008JF001036.

Kavanaugh, J. L., and G. K. C. Clarke (2000), Evidence for extreme pressure pulses in the subglacial water system, *J. Glaciol.*, *46*, 206–212, doi:10.3189/172756500781832963.

Kennedy, F. E., E. M. Schulson, and D. E. Jones (2000), The friction of ice on ice at low sliding velocities, *Philos. Mag. A*, *80*(5), 1093–1110, doi:10.1080/01418610008212103.

Kirkbride, M., and N. Spedding (1996), The influence of englacial drainage on sediment transport pathways and till texture of temperate valley glaciers, *Ann. Glaciol.*, *22*, 160–166.

Lambe, T. W., and R. V. Whitman (1969), *Soil Mechanics*, Wiley, New York.

Lliboutry, L. (2002), Overthrusts due to easy-slip/poor-slip transitions at the bed: The mathematical singularity with non-linear isotropic viscosity, *J. Glaciol.*, *48*, 109–117, doi:10.3189/172756502781831700.

Maeno, N., and M. Arakawa (2004), Adhesion shear theory of ice friction at low sliding velocities, combined with ice sintering, *J. Appl. Phys.*, *95*(1), 134–139, doi:10.1063/1.1633654.

Moore, P. L., N. R. Iverson, K. A. Brugger, T. S. Hooyer, D. Cohen, and P. Jansson (2008), Frozen margin dynamics at Storglaciären, Sweden, *Eos Trans. AGU*, *89*(53), Fall Meet., Suppl., Abstract C11D–0526.

Moore, P. L., N. R. Iverson, and D. Cohen (2009), Ice flow across a warm-based/cold-based transition at a glacier margin, *Ann. Glaciol.*, *50*(52), 1–8.

Murray, T., J. Dowdeswell, D. J. Drewry, and I. Frearson (1998), Geometric evolution and ice dynamics during a surge of Bakaninbreen, Svalbard, *J. Glaciol.*, *44*, 263–272.

Palmer, A. C., and J. R. Rice (1973), The growth of slip surfaces in the progressive failure of over-consolidated clay, *Proc. R. Soc. London, Ser. A*, *332*(1591), 527–548, doi:10.1098/rspa.1973.0040.

Paterson, W. S. B. (1994), *Physics of Glaciers*, 3rd ed., Pergamon, Tarrytown, N. Y.

Pfeffer, W. T. (1987), Structure and deformation in a propagating surge front, Ph.D. dissertation, Univ. of Wash., Seattle.

Pfeffer, W. T. (1992), Stress-induced foliation in the terminus of Variegated Glacier, Alaska, U.S.A., formed during the 1982–1983 surge, *J. Glaciol.*, *38*, 213–222.

Rabus, B. T., and K. A. Echelmeyer (1997), The flow of a polythermal glacier; McCall Glacier, Alaska, USA, *J. Glaciol.*, *43*, 522–536.

Raymond, C. F., T. Johansnesson, and T. Pfeffer (1987), Propagation of a glacier surge into stagnant ice, *J. Geophys. Res.*, *92*(B9), 9037–9049, doi:10.1029/JB092iB09p09037.

Renshaw, C. E., and E. M. Schulson (2001), Universal behaviour in compressive failure of brittle materials, *Nature*, *412*, 897–900, doi:10.1038/35091045.

Rist, M. A., and S. A. F. Murrell (1994), Ice triaxial deformation and fracture, *J. Glaciol.*, *40*, 305–318.

Scholz, C. H. (2002), *Mechanics of Earthquakes and Faulting*, Cambridge Univ. Press, Cambridge, U. K.

Schulson, E. M. (2001), Brittle failure of ice, *Eng. Fract. Mech.*, *68*, 1839–1887, doi:10.1016/S0013-7944(01)00037-6.

Sharp, M., W. Lawson, and R. S. Anderson (1988), Tectonic processes in a surge-type glacier, *J. Struct. Geol.*, *10*, 499–515, doi:10.1016/0191-8141(88)90037-5.

Smith, A. M., T. Murray, B. M. Davison, A. F. Clough, J. Woodward, and H. Jiskoot (2002), Late surge glacial conditions on Bakaninbreen, Svalbard, and implications for surge termination, *J. Geophys. Res.*, *107*(B8), 2152, doi:10.1029/2001JB000475.

Szabo, D., and M. Schneebeli (2007), Subsecond sintering of ice, *Appl. Phys. Lett.*, *90*, 151916, doi:10.1063/1.2721391.

Weertman, J. (1961), Mechanism for the formation of inner moraines found near the edge of cold ice caps and ice sheets, *J. Glaciol.*, *3*, 965–978.

Woodward, J., T. Murray, and A. McCaig (2002), Formation and reorientation of structure in the surge-type glacier Kongsvegen, Svalbard, *J. Quat. Sci.*, *17*(3), 201–209, doi:10.1002/jqs.673.

Woodward, J., T. Murray, and A. McCaig (2003), Reply, *J. Quat. Sci.*, *18*(1), 99–100, doi:10.1002/jqs.736.

D. Cohen, N. R. Iverson, and P. L. Moore, Department of Geological and Atmospheric Sciences, Iowa State University, Ames, IA 50011, USA. (pmoore@iastate.edu)